The response of mesophyll conductance to short-term variation in CO2 in the C4 plants Setaria viridis and Zea mays

Nerea Ubierna, Anthony Gandin, Asaph Cousins

Journal of Experimental Botany, Vol. 69, No. 5 pp. 1159–1170, 2018
doi:10.1093/jxb/erx464 Advance Access publication 21 February 2018
This paper is available online free of all access charges (see http://jxb.oxfordjournals.org/open_access.html for further details)

RESEARCH PAPER

The response of mesophyll conductance to short-term variation in CO_2 in the C_4 plants *Setaria viridis* and *Zea mays*

Nerea Ubierna[1], Anthony Gandin[1,†] and Asaph B. Cousins[1,*]

[1] School of Biological Sciences, Molecular Plant Sciences, Washington State University, Pullman, Washington 99164–4236, USA

[†] Present address: Université de Lorraine, Faculté des Sciences et Techniques, Ecologie et Ecophysiologie Forestières, F54506 Vandoeuvre Les Nancy, France.

* Correspondence: acousins@wsu.edu

Received 26 March 2017; Editorial decision 4 December 2017; Accepted 10 January 2018

Editor: Susanne von Caemmerer, Australian National University, Australia

Abstract

Mesophyll conductance (g_m) limits rates of C_3 photosynthesis but little is known about its role in C_4 photosynthesis. If g_m were to limit C_4 photosynthesis, it would likely be at low CO_2 concentrations (pCO_2). However, data on C_4-g_m across ranges of pCO_2 are scarce. We describe the response of C_4-g_m to short-term variation in pCO_2, at three temperatures in *Setaria viridis*, and at 25 °C in *Zea mays*. Additionally, we quantified the effect of finite g_m calculations of leakiness (ϕ) and the potential limitations to photosynthesis imposed by stomata, mesophyll, and carbonic anhydrase (CA) across pCO_2. In both species, g_m increased with decreasing pCO_2. Including a finite g_m resulted in either no change or increased ϕ compared with values calculated with infinite g_m depending on whether the observed ^{13}C discrimination was high (*Setaria*) or low (*Zea*). Post-transitional regulation of the maximal PEP carboxylation rate and PEP regeneration limitation could influence estimates of g_m and ϕ. At pCO_2 below ambient, the photosynthetic rate was limited by CO_2 availability. In this case, the limitation imposed by the mesophyll was similar or slightly lower than stomata limitation. At very low pCO_2, CA further constrained photosynthesis. High g_m could increase CO_2 assimilation at low pCO_2 and improve photosynthetic efficiency under situations when CO_2 is limited, such as drought.

Keywords: *A*-C_i curves, carbonic anhydrase, CO_2, C_4 photosynthesis, diffusional limitations, *in-vitro* V_{pmax}, leakiness, mesophyll conductance, *Setaria viridis*, *Zea mays*.

Introduction

In C_4 plants photorespiration is reduced by concentrating CO_2 around Rubisco (ribulose 1,5-bisphosphate carboxylase/oxygenase) (Edwards and Walker, 1983; Hatch, 1987; Sage, 2004). In Kranz-type C_4 plants this is achieved with a compartmentalized two-carboxylation process: (1) in the cytosol of mesophyll cells, bicarbonate (HCO_3^-) and phospho*enol*pyruvate are fixed into four-carbon acids by phospho*enol*pyruvate carboxylase (PEPC) (Hatch *et al.*, 1967); and (2) in chloroplasts of the bundle-sheath cells the concentrated CO_2 released from the decarboxylation of these acids is fixed by Rubisco.

Mesophyll conductance (g_m) describes the movement of CO_2 from stomata across the intercellular spaces to the sites of first carboxylation, which are the chloroplast stroma or mesophyll cytosol in C_3 and C_4 species, respectively (Evans and von Caemmerer, 1996). There is extensive research describing g_m in C_3 species; however, C_4-g_m is poorly understood because it is difficult to estimate. Traditionally g_m was assumed to be larger in C_4 compared to C_3 species, but most recent studies suggest that values for C_4-g_m correspond to higher-end C_3-g_m reports, and that C_4-g_m reacts similarly to C_3-g_m with

regards to variation in factors such as leaf age and temperature (Barbour *et al.*, 2016; Osborn *et al.*, 2017; Ubierna *et al.*, 2017). If C_4-g_m is lower than previously thought, that could affect derivations of other key parameters such as leakiness (ϕ, the proportion of C fixed by PEPC that subsequently leaks out the bundle-sheath cells). Leakiness cannot be directly measured and is commonly estimated from observations and models of ^{13}C discrimination ($\Delta^{13}C$) (Farquhar, 1983; Farquhar and Cernusak, 2012). Historically, g_m is generally assumed to be infinite when solving for ϕ from $\Delta^{13}C$; however, this simplification and estimates of ϕ would be compromised if g_m is finite and low.

Mesophyll conductance has long been recognized as a significant limitation for C_3 photosynthesis (Evans, 1983; Evans *et al.*, 1986; Evans and Terashima, 1988), limiting photosynthesis as much as stomatal conductance (Warren, 2008). It is unclear if g_m limits C_4 photosynthesis as the reduction of photorespiration achieved by the CO_2-concentrating mechanism saturates C_4 photosynthesis at ambient pCO_2. If g_m were to limit C_4 photosynthesis, it would likely only be at very low pCO_2. However, not much is known about the variation of C_4-g_m with pCO_2. In the C_4 grass *Setaria viridis*, g_m derived with the ^{18}O discrimination ($\Delta^{18}O$) method increased as pCO_2 decreased, although the variation was not significant (Osborn *et al.*, 2017). Some reports have shown that in C_3 species g_m increases with short-term exposure to decreasing pCO_2 (Bongi and Loreto, 1989; Loreto *et al.*, 1992; Flexas *et al.*, 2007, 2008; Hassiotou *et al.*, 2009; Bunce, 2010; Douthe *et al.*, 2011; Tazoe *et al.*, 2011). However, others have suggested that C_3-g_m is insensitive to changes in pCO_2 (Loreto *et al.*, 1992; Tazoe *et al.*, 2009). It has been hypothesized that the observed C_3-g_m response to pCO_2 might result from a significant chloroplast resistance (Tholen and Zhu, 2011; Tholen *et al.*, 2012) or artifacts in the calculations (Gu and Sun, 2014).

In C_4 plants, g_m has been estimated with the $\Delta^{18}O$ method (Gillon and Yakir, 2000*a*, 2000*b*; Barbour *et al.*, 2016; Osborn *et al.*, 2017; Ubierna *et al.*, 2017) and the *in vitro* maximal PEP carboxylation rate (V_{pmax}) method (Ubierna *et al.*, 2017). The latter method solves for the pCO_2 in the mesophyll cells (C_m) needed to simultaneously match modeled and measured rates of CO_2 assimilation and $\Delta^{13}C$ when the models are parameterized with *in vitro* V_{pmax}, as determined in a crude leaf extract. Values derived for g_m with the $\Delta^{18}O$ and *in vitro* V_{pmax} methods were similar in two C_4 species measured over a range of temperatures (Ubierna *et al.*, 2017). The *in vitro* V_{pmax} method also allows the implementation of two modeling alternatives: carbonic anhydrase (CA)-saturated and CA-limited. They differ in the calculation of PEP carboxylation rate as a function of CO_2 or HCO_3^- for the CA-saturated and -limited scenarios, respectively. Ubierna *et al.* (2017) found no difference between CA-limited and CA-saturated estimates of g_m at ambient pCO_2, but CA limitation is expected at low pCO_2.

In this study, we calculated g_m using the *in vitro* V_{pmax} method across a range of pCO_2 in two C_4 grasses, one economically important (*Zea mays*) and the other the adopted model system for studying C_4 photosynthesis (*S. viridis*). Measurements were performed at three temperatures (10, 25, and 40 °C) in *Setaria* and at 25 °C in *Zea*. Our objectives were to: (1) describe the response of C_4-g_m to short-term variation in pCO_2; (2) evaluate the impact of disequilibrium between CO_2 and HCO_3^- at a range of pCO_2 and temperatures; (3) investigate if g_m represents a limitation to C_4 photosynthesis across pCO_2; and (4) assess the impact of finite g_m on ϕ calculations.

Materials and methods

Plant material

Seeds of *Z. mays* (var. Trucker's Favorite, Victory Seed Company, Oregon, USA) were grown in a greenhouse supplemented with artificial lighting at the School of Biological Sciences at Washington State University, Pullman, WA (USA) during August to October 2011. Seeds of *S. viridis* (A-010) were grown in a controlled environment growth chamber (Enconair Ecological GC-16) in 2013. Plants used for measurements were 4 and 6 weeks old for *Zea* and *Setaria*, respectively. *Zea* was fertilized with 17-3-6 NPK and weekly additions of 4 g l^{-1} solution of 10% Fe-DPTA (Sprint 330, Becker Underwood, IA, USA). *Setaria* was treated weekly with Peters 20-20-20 (J. R. Peters, Inc., Allentown, PA, USA). For all plants, the photon flux density was ≥500 µmol m^{-2} s^{-1}, the day length was 14 h, and the temperature was 25–28/20–25 °C for day/night.

Coupled gas exchange and isoflux measurements

The system used for measurements has been described in detail in Ubierna *et al.* (2013, 2017). Briefly, a LI-6400XT open gas exchange system assembled with a 6400-22L conifer chamber fitted with a LI-6400–18 RGB light source (Li-Cor, Lincoln, NE, USA) was coupled with a tunable-diode laser absorption spectroscope (TDLAS, TGA 200A, Campbell Scientific, Inc. Logan, UT, USA). The entire gas exchange system was placed in a growing cabinet (Percival Scientific, Perry, IA), where the temperature was varied to match leaf temperature (T_L) settings. The TDLAS data were calibrated with the concentration series method (Tazoe *et al.*, 2011; Ubierna *et al.*, 2013) using two calibration gases, one measured at different [CO_2] that spanned the gas exchange reference and sample lines. Each measurement cycle included five to seven TDLAS sequences of zero air, calibration gases, reference, and sample lines measured for 40 s each. Data from the last three sequences were averaged and used for calculations.

Young fully-expanded leaves of *Setaria* and *Zea* were acclimated for ~1 h with chamber conditions of C_a (ambient CO_2 supply to the chamber) ≈ 35 Pa, 21% O_2, and photosynthetically active radiation (PAR) =2000 µmol m^{-2} s^{-1}. Then, C_a was varied in steps, and gas and ^{13}C isotopic exchange were measured simultaneously. In *Setaria* (n=4) C_a was set at 5, 7, 10, 12, 14, 19, 28, 38, 56, and 93 Pa, and measurements were performed at T_L=10, 25 and 40 °C. In *Zea* (n=3), C_a was set at 9, 14, 19, 35, 56, 84, and 112 Pa, and T_L=25 °C. In both species the measurements were performed in the sequence ambient – low – ambient – high pCO_2.

Enzyme-limited C_4 photosynthesis model for CA-limited or CA-saturated conditions

The enzyme-limited C_4 photosynthesis rate is (von Caemmerer, 2000):

$$A = \frac{-b - \sqrt{b^2 - 4ac}}{2a}, \qquad \text{Eqn 1}$$

where:

$$a = 1 - \frac{\alpha}{u_{oc}} \frac{K_c}{K_o}, \qquad \text{Eqn 2}$$

$$b = -\left[\begin{array}{l} V_p - R_m + g_{bs}C_m + V_{cmax} - R_d \\ +g_{bs}K_c\left(1+\frac{O_m}{K_o}\right)+\frac{\alpha}{u_{oc}}\left(\gamma^* V_{cmax} + R_d\frac{K_c}{K_o}\right)\end{array}\right], \quad \text{Eqn 3}$$

$$\begin{array}{l} c = \left(V_{cmax} - R_d\right)\left(V_p - R_m + g_{bs}C_m\right) \\ -V_{cmax}g_{bs}\gamma^* O_m - R_d g_{bs}K_c\left(1+\frac{O_m}{K_o}\right),\end{array} \quad \text{Eqn 4}$$

where α (= 0) is the fraction of PSII activity in the bundle-sheath cells (von Caemmerer, 2000); u_{oc} is the ratio of O_2 and CO_2 diffusivities and solubilities, 0.047 at 25 °C but variable with temperature (Yin *et al.*, 2016); g_{bs} is the bundle-sheath conductance, 0.0164 µmol m^{-2} s^{-1} Pa^{-1} (Ubierna *et al.*, 2013) or variable; O_m is the O_2 partial pressure in the mesophyll (19.5 kPa, which corresponds to 21%); R_d is the non-photorespiratory CO_2 released in the dark, assumed to equal measured rates of dark respiration after 30 min of dark adaptation, which at 25 °C were 1.89 and 1.06 µmol m^{-2} s^{-1} in *Zea* and *Setaria*, respectively, but were also measured at each temperature; R_m is the mesophyll mitochondrial respiration rate, R_m=0.5R_d (von Caemmerer, 2000); γ* is half of the reciprocal of Rubisco specificity, and equals 0.5/$S_{C/O}$ (von Caemmerer, 2000), where $S_{C/O}$ is the Rubisco CO_2/O_2 specificity. K_C and K_O are the Michaelis–Menten constants of Rubisco for CO_2 and O_2, respectively. $S_{C/O}$, K_C, and K_O were determined *in vitro* at 25 °C in *Zea* ($S_{C/O}$=2147 Pa Pa^{-1}, K_C=96 Pa, K_O=49 683 Pa; R.A. Boyd, Washington State University, pers. comm.) and *Setaria* ($S_{C/O}$=1310 Pa Pa^{-1}, K_C=121 Pa, K_O=29 200 Pa; Boyd *et al.*, 2015). Their values at different temperatures were obtained using the temperature functions of Boyd *et al.* (2015). For V_{cmax} (maximal Rubisco carboxylation rate) we used *in vivo* values calculated as described in Ubierna *et al.* (2017) or as specified otherwise. The calculation of C_m (pCO_2 in the mesophyll cells) will be discussed subsequently.

CA-saturated and CA-limited models differ as follows.

(1) The calculation of PEP carboxylation rate (V_p):

$$V_p = \left\{\begin{array}{l} \text{CA saturated} \rightarrow \frac{C_m V_{pmax}}{C_m + K_p} \\ \text{CA limited} \rightarrow \frac{\left[HCO_3^-\right]V_{pmax}}{\left[HCO_3^-\right]+K_p}\end{array}\right\}, \quad \text{Eqn 5}$$

where the maximal PEP carboxylation rate (V_{pmax}) was measured *in vitro* at 25 °C in *Zea* (184 µmol m^{-2} s^{-1}, R. A. Boyd, pers. comm.) and in *Setaria* (450 µmol m^{-2} s^{-1}, Boyd *et al.* 2015) and varied with temperature as described in Boyd *et al.* (2015). For all species, the Michaelis–Menten constant of PEPC for CO_2 (K_P) was modeled with the temperature response and value at 25 °C (60.5 µM HCO_3^-) from Boyd *et al.* (2015). The [HCO_3^-] was calculated as previously discussed (Jenkins *et al.*, 1989; Hatch and Burnell, 1990; Boyd *et al.*, 2015): for details see Ubierna *et al.* (2017).

If the rate of PEP regeneration is limiting, then V_p is (von Caemmerer, 2000):

$$V_p = \min\left(V_p \text{ calculated with Eqn 5}, V_{pr}\right), \quad \text{Eqn 6}$$

where V_{pr} is the PEP regeneration rate (Peisker, 1986; Peisker and Henderson, 1992). We arbitrarily set V_{pr} to 64 and 59 µmol m^{-2} s^{-1} in *Setaria* and *Zea*, respectively, which corresponded to twice the maximum measured net assimilation rate, A.

(2) The calculation of the ratio V_p/V_h, where V_h is hydration rate:

$$\frac{V_p}{V_h} = \left\{\begin{array}{l} \text{CA saturated} \rightarrow 0 \\ \text{CA limited} \rightarrow \frac{V_p}{C_m K_{CA}}\end{array}\right\}, \quad \text{Eqn 7}$$

where K_{CA} is the rate constant of CA for CO_2, that at 25 °C was 65.5 and 124 µmol m^{-2} s^{-1} Pa^{-1} in *Zea* and *Setaria*, respectively (R.A. Boyd pers. comm., Boyd *et al.*, 2015), varying with temperature as described in Boyd *et al.* (2015).

Measurements and models of discrimination

The observed photosynthetic discrimination against ^{13}C (Δ^{13}_{obs}) is calculated as (Evans *et al.*, 1986):

$$\Delta^{13}_{obs} = \frac{\frac{C_{in}}{C_{in}-C_{out}}\left(\delta_{out}-\delta_{in}\right)}{1+\delta_{out}-\frac{C_{in}}{C_{in}-C_{out}}\left(\delta_{out}-\delta_{in}\right)}, \quad \text{Eqn 8}$$

where C and δ are the $^{12}CO_2$ mol fraction and the $\delta^{13}C$ of the CO_2, respectively, in dry air in and out the chamber.

The theoretical model for $\Delta^{13}C$ is (Farquhar and Cernusak, 2012):

$$\begin{array}{l} \Delta^{13}_{theo} = \frac{1}{1-t}\left[a_b\frac{C_a - C_L}{C_a} + a_s\frac{C_L - C_i}{C_a}\right] \\ +\frac{1+t}{1-t}\left[a_m\frac{C_i - C_m}{C_a} + \frac{b_4 + \phi\left(\frac{b_3 C_{bs}}{C_{bs}-C_m} - s\right)}{1+\frac{\phi C_m}{C_{bs}-C_m}}\frac{C_m}{C_a}\right].\end{array} \quad \text{Eqn 9}$$

Values and calculations of the variables included in this equation have been discussed before (i.e. Ubierna *et al.*, 2017) and can also be found in Supplementary Methods S1 at *JXB* online.

Calculation of mesophyll conductance (g_m)

Following Fick's law of diffusion:

$$g_m = \frac{A}{C_i - C_m}, \quad \text{Eqn 10}$$

where the C_m is calculated for two case scenarios, CA-saturated and CA–limited, resulting in CA-sat g_m and CA-lim g_m values. In both cases, C_m is derived with the *in vitro* V_{pmax} method as the C_m that needs to be combined with *in vitro* V_{pmax} to match measurements and predictions of A and $\Delta^{13}C$ (Eqns 1, 9); details on these calculations have been provided in Ubierna *et al.* (2017). The CA-sat and CA-lim options are introduced through the calculation of V_p and V_p/V_h (Eqns 5–7).

Limitations to photosynthesis

To calculate the limitation on CO_2 assimilation by either finite stomatal conductance (L_s), by mesophyll conductance (L_m), or by carbonic anhydrase (L_{CA}), we adapted to C_4 photosynthesis an approach previously used for C_3 photosynthesis. This compares A when all conductances are finite with the A estimated assuming that the conductance related with the limitation of interest is infinite (Farquhar and Sharkey, 1982; Warren *et al.*, 2003). In all cases A was calculated with Eqn 1 and assuming:

(a) A_{all} (expected A with all limitations, ≈ measured photosynthetic rate): finite g_s and g_m, CA-lim model.

(b) A_s (expected A if there were no stomatal limitations): infinite g_s (C_i=C_a), finite g_m, CA-lim model.

(c) A_m (expected A if there were no mesophyll limitations): infinite g_m (C_m=C_i), g_s as measured, CA-lim model.

(d) A_{CA} (expected A if there were no CA limitations): g_s as measured, g_m finite, CA-sat model.

Then L_s, L_m, and L_{CA} were calculated as:

$$L_s = 100 \times \frac{A_s - A_{all}}{A_s}, \quad \text{Eqn 11}$$

$$L_m = 100 \times \frac{A_m - A_{all}}{A_m}, \quad \text{Eqn 12}$$

$$L_{CA} = 100 \times \frac{A_{CA} - A_{all}}{A_{CA}}. \quad \text{Eqn 13}$$

Calculation of leakiness (ϕ)

The C_4 photosynthesis model (von Caemmerer, 2000) calculates ϕ as:

$$\phi = \frac{g_{bs}(C_{bs} - C_m)}{V_p}, \quad \text{Eqn 14}$$

where C_{bs}, the pCO_2 in the bundle-sheath cells, is (von Caemmerer, 2000):

$$C_{bs} = \frac{\gamma^* O_s + K_C\left(1 + \frac{O_s}{K_o}\right)\left(\frac{A + R_d}{V_{cmax}}\right)}{1 - \frac{A + R_d}{V_{cmax}}} = C_m + \frac{V_p - A - R_m}{g_{bs}}, \quad \text{Eqn 15}$$

where O_s is the O_2 partial pressure in the bundle-sheath cells.

From $\Delta^{13}C$ (Eqn 9), ϕ is solved as:

$$\phi_1 = \frac{C_{bs} - C_m}{C_m} \times \frac{\begin{array}{c}\Delta^{13}_{obs}(1-t)C_a - \bar{a}(C_a - C_i) \\ -a_m(C_i - C_m)(1+t) - b_4(1+t)C_m \end{array}}{\begin{array}{c}(1+t)\left[b_3 C_{bs} - s(C_{bs} - C_m) + a_m(C_i - C_m)\right] \\ +\bar{a}(C_a - C_i) - C_a\Delta^{13}_{obs}(1-t)\end{array}}, \quad \text{Eqn 16}$$

where b_3 (combined effects of Rubisco fractionation, and fractionations associated with respiration and photorespiration) and b_4 (combined fractionation during PEP carboxylation, hydration, and respiration) are calculated as (Farquhar, 1983; Cousins *et al.*, 2006):

$$b_3 \cong b_3' - \frac{eR_d}{V_c} - \frac{0.5 f V_o}{V_c}, \quad \text{Eqn 17}$$

$$b_4 = b_4'\left(1 - \frac{V_p}{V_h}\right) + (e_s + h)\frac{V_p}{V_h} - \frac{eR_m}{V_p}. \quad \text{Eqn 18}$$

A description of other variables included in Eqns 16–19 can be found in Supplementary Methods S1.

To evaluate the effect of g_m on calculations of ϕ we implemented four model scenarios, which differed in values for g_m, calculation of V_p, or constrains imposed. Model 1 used *in vitro* V_{pmax} and g_m finite and equal to the values for CA-lim g_m presented in the Results; Model 2 used *in vivo* V_{pmax} and g_m infinite; Model 3 was the same as Model 1 but the solution was only constrained by A and not $\Delta^{13}C$; and Model 4 was the same as Model 1 but with V_p calculated with Eqn 6, which introduces a PEP regeneration limitation. The *in vitro* V_{pmax} method calculates g_m by solving the system of two equations formed by the models of A and $\Delta^{13}C$. Therefore, once a solution is found, ϕ values calculated with either Eqn 14 or 16 are identical. This is the case for Models 1, 2, and 4; however, in Model 3, which is constrained only by A, ϕ was obtained only with Eqn 14. All four modeling scenarios described above used the CA-limited calculations (Eqns 5–7).

At ambient pCO_2, ϕ was also calculated with a simplified equation derived from $\Delta^{13}C$ assuming that C_{bs} is much larger than C_m and that hydration and assimilation fluxes are large ($V_p/V_h \approx 0$, and $V_o \approx 0$, where V_o is oxygenation rate):

$$\phi_2 = \frac{\frac{\Delta_{obs}(1-t)C_a - \bar{a}(C_a - C_i)}{1+t} - a_m C_i + C_m\left(a_m - \overline{b_4}\right)}{C_m\left(\overline{b_3} - s\right)}, \quad \text{Eqn 19}$$

where $\overline{b_3}$ and $\overline{b_4}$ are (von Caemmerer *et al.*, 2014):

$$\overline{b_3} = b_3' - \frac{eR_d}{A + R_d} + \frac{e0.5R_d}{A + 0.5R_d}, \quad \text{Eqn 20}$$

$$\overline{b_4} = b_4' - \frac{e0.5R_d}{A + 0.5R_d}. \quad \text{Eqn 21}$$

Statistical analyses

Statistical analyses were performed using SAS v9.4 (SAS Institute Inc., Cary, NC, USA). Differences between CA-lim g_m and CA-sat g_m were investigated using *t*-tests (H_o: CA-lim g_m/CA-sat g_m=1). The effect of CO_2 supply on CA-lim g_m was analysed using repeated measurements ANOVA. Data were log-transformed to meet normality criteria. In *Setaria* we used PROC MIXED with: *plant* as the repeated measurement; pCO_2, *temperature*, and their interaction as fixed effects; a covariance structure of compound symmetry; and we applied Kenward–Roger's approximation to correct the denominator degrees of freedom (Arnau *et al.*, 2009). In *Zea*, we used PROC ANOVA with the statement REPEAT.

Results

A-C_i curves and observed ^{13}C photosynthetic discrimination

Under all leaf measurement temperatures (T_L), the rate of net photosynthesis (A) in *Setaria* increased with C_i as the pCO_2 supplied increased from ~5 Pa to ambient air values (~35 Pa) and then leveled off (Fig. 1A). At all pCO_2, increasing T_L resulted in larger A (Fig. 1A). In *Zea*, A also increased with increasing C_i and reached a maximum at ambient air pCO_2 before decreasing at higher pCO_2 (Fig. 1B).

At ambient air pCO_2 and 25 °C, Δ^{13}_{obs} was larger in *Setaria* (4.5 ± 0.1‰) than in *Zea* (3.1 ± 0.2‰) (Fig. 1C, D). In *Zea*, the Δ^{13}_{obs} was low at ambient air pCO_2 and increased at lower or higher C_i (Fig. 1D). However, in *Setaria*, Δ^{13}_{obs} remained constant with C_i when T_L=25 °C, but decreased as C_i increased both at 40 and 10 °C (Fig. 1C).

Mesophyll conductance calculated assuming CA-saturated or CA-limited conditions

For both species and at all temperatures, the ratio CA-lim g_m/CA-sat $g_m \approx 1$ when pCO_2 was above ambient (Fig. 2). As pCO_2 decreased, CA-lim g_m became larger than CA-sat g_m; the differences increased with temperature and were larger in *Zea* than in *Setaria*. In *Setaria*, CA-lim g_m and CA-sat g_m were significantly different (P<0.05) at all pCO_2 at 40 °C, at all pCO_2 except at ambient and the measurement just above

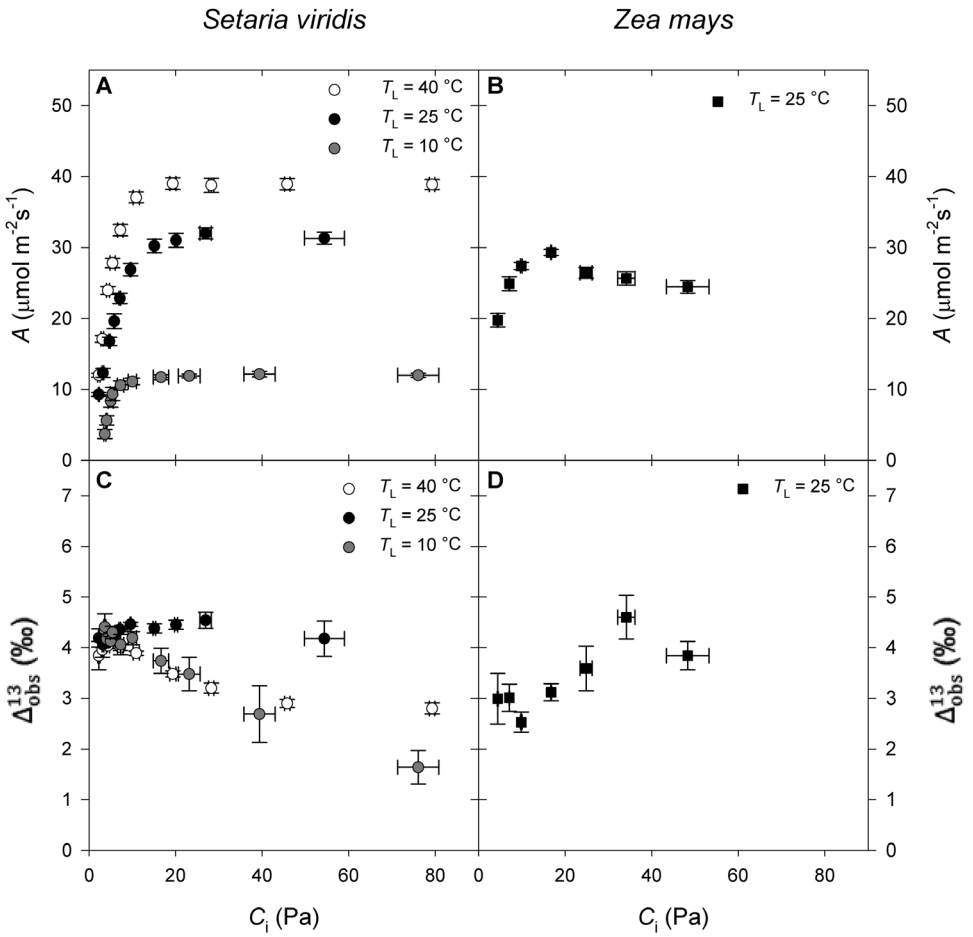

Fig. 1. Responses of (A, B) photosynthetic rate (*A*) and (C, D) observed ^{13}C photosynthetic discrimination (Δ^{13}_{obs}) to variation in the CO_2 partial pressure inside the leaf (C_i) in *Setaria viridis* (circles) and *Zea mays* (squares). In *Setaria*, three leaf temperatures (T_L) were measured: 40, 25, and 10 °C, as indicated in the key. Measurements in *Zea* were at T_L=25 °C. Values are means ±SE; *n*=4 in *Setaria* and *n*=3 in *Zea*.

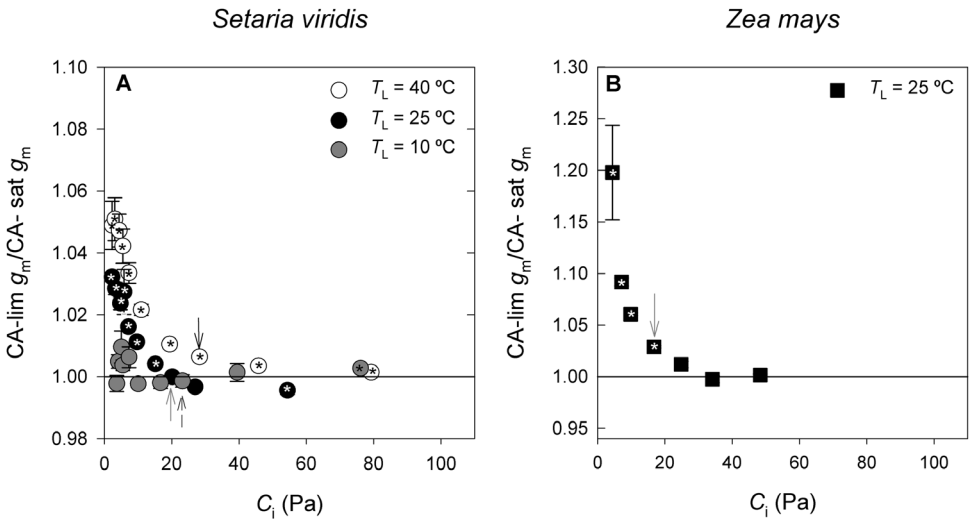

Fig. 2. The ratio of carbonic anhydrase-limited mesophyll conductance (CA-lim g_m) to CA-saturated g_m (CA-sat g_m) at different pCO_2 inside the leaf (C_i) in (A) *Setaria viridis* (circles) and (B) *Zea mays* (squares). *Setaria* was measured at three leaf temperatures (T_L): 40, 25, and 10 °C, as indicated in the key. *Zea* was measured at T_L=25 °C. Values are means ±SE; *n*=4 in *Setaria* and *n*=3 in *Zea*. An asterisk inside a symbol indicates CA-lim g_m/CA-sat $g_m \neq 1$ with P<0.05. The arrows indicate the values at ambient pCO_2 and at 40 °C (black arrow), 25 °C (grey arrow), and 10 °C (dashed arrow).

ambient at 25 °C, and at the largest pCO_2 at 10 °C (Fig. 2A). In *Zea*, CA-lim g_m and CA-sat g_m were significantly different (P<0.05) at all pCO_2≤ambient air (Fig. 2 B).

In *Setaria*, the under-estimation of g_m by ignoring the CA limitation was very small (maximum of 5%, CA-lim g_m/CA-sat g_m<1.1; Fig. 2A). However, in *Zea*, the CA-lim g_m

calculated at the lowest pCO_2 was 20 ± 8% larger than CA-sat g_m at 25 °C. Because CA limitation was relevant at low pCO_2, for subsequent analyses we use the CA-lim g_m values for all species, temperatures, and pCO_2.

CO_2 response of mesophyll conductance

The CA-lim g_m significantly increased as pCO_2 decreased in *Setaria* at all temperatures (P<0.0001) and in *Zea* at 25 °C (P<0.0004) (Fig. 3). At ambient pCO_2 and 25 °C, CA-lim g_m values (mean±SE) were 2.00 ± 0.10 µmol m^{-2} s^{-1} Pa^{-1} in *Setaria*, and 2.43 ± 0.13 µmol m^{-2} s^{-1} Pa^{-1} in *Zea*. At the lowest pCO_2 measured (~5–9 Pa) and 25 °C, the CA-lim g_m increased to 6.30 ± 0.32 and 16.20 ± 5.74 µmol m^{-2} s^{-1} Pa^{-1} in *Setaria* and *Zea*, respectively. Values for C_m across C_i can be found in Supplementary Fig. S1.

To compare the magnitude of the change in CA-lim g_m across species and temperatures, CA-lim g_m was normalized by dividing each value at a given temperature and pCO_2 by CA-lim g_m at ambient pCO_2 at that temperature (Fig. 3 D–F). At 25 °C, the increase in CA-lim g_m with decreasing pCO_2 was steeper in *Zea* than in *Setaria* (Fig. 3E). In *Setaria*, the g_m pCO_2 response was greatest at 40 °C and there was little difference between the 25 and 10 °C curves.

Limitations to photosynthesis

At elevated pCO_2 assimilation rate was not limited by diffusion or substrate availability, as indicated by L_s, L_m, and L_{CA} ≈ 0% for both species and all temperatures (Fig. 4). However, below ambient pCO_2, the diffusional limitation to A increased exponentially with decreasing pCO_2. The data in Fig. 4 show the different limitations as a function of the amount of substrate available: C_a, C_i, and C_m for L_s, L_m, and L_{CA}, respectively. In *Setaria*, diffusional limitations were lower at 10 °C than at any other temperature. Comparing *Zea* and *Setaria* at 25 °C, they had similar L_s but L_m was larger in *Setaria* than in *Zea*. For example, when C_a=9 Pa, L_s=23% and 19% in *Setaria* and *Zea*, respectively. The corresponding C_i at this C_a was 5 Pa for both species, whereas L_m was almost double in *Setaria* (23%) compared to *Zea* (12%) (Fig. 4C, D). In both species, L_{CA} was small in comparison with L_s and L_m, and rapidly decreased below 5% as pCO_2 increased.

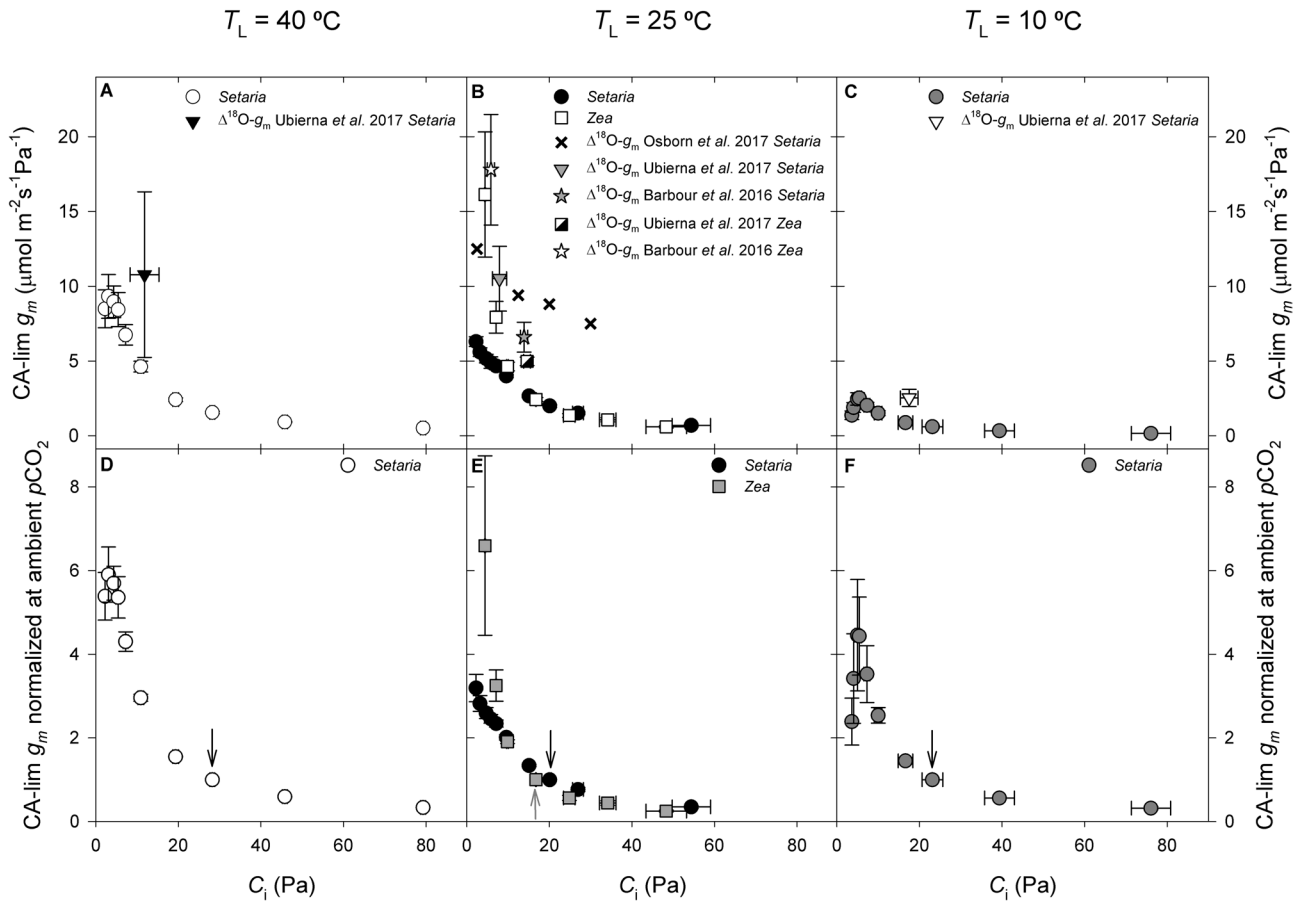

Fig. 3. The response of carbonic anhydrase-limited mesophyll conductance (CA-lim g_m) to changes in pCO_2 inside the leaf (C_i) in (A, C) *Setaria viridis* (circles) and (B) *Zea mays* (white squares). *Setaria* was measured at three leaf temperatures, as indicated at the top of the figure. *Zea* was measured at T_L=25 °C. For comparison, the available literature reports for $\Delta^{18}O$-g_m for different species and temperatures are included, as indicated in the keys: Ubierna *et al.* (2017) *Setaria* measured at T_L=40 °C, T_L=25 °C, and T_L=10 °C; Osborn *et al.* (2017) *Setaria* measured at T_L=25 °C; Barbour *et al.* (2016) *Setaria* measured with block temperature of 30 °C; Ubierna *et al.* (2017) *Zea* measured at T_L=25 °C; Barbour *et al.* (2016) *Zea* measured with block temperature of 30 °C. For all species and temperatures CA-lim g_m significantly varied with pCO_2. (D–F) The CO_2 response of normalized g_m, calculated by dividing individual values by the g_m at ambient pCO_2 at each temperature. Values are means ±SE; n=4 in *Setaria*, n=3 in *Zea*. The arrows indicate the values at ambient pCO_2: black, *Setaria*; grey, *Zea*.

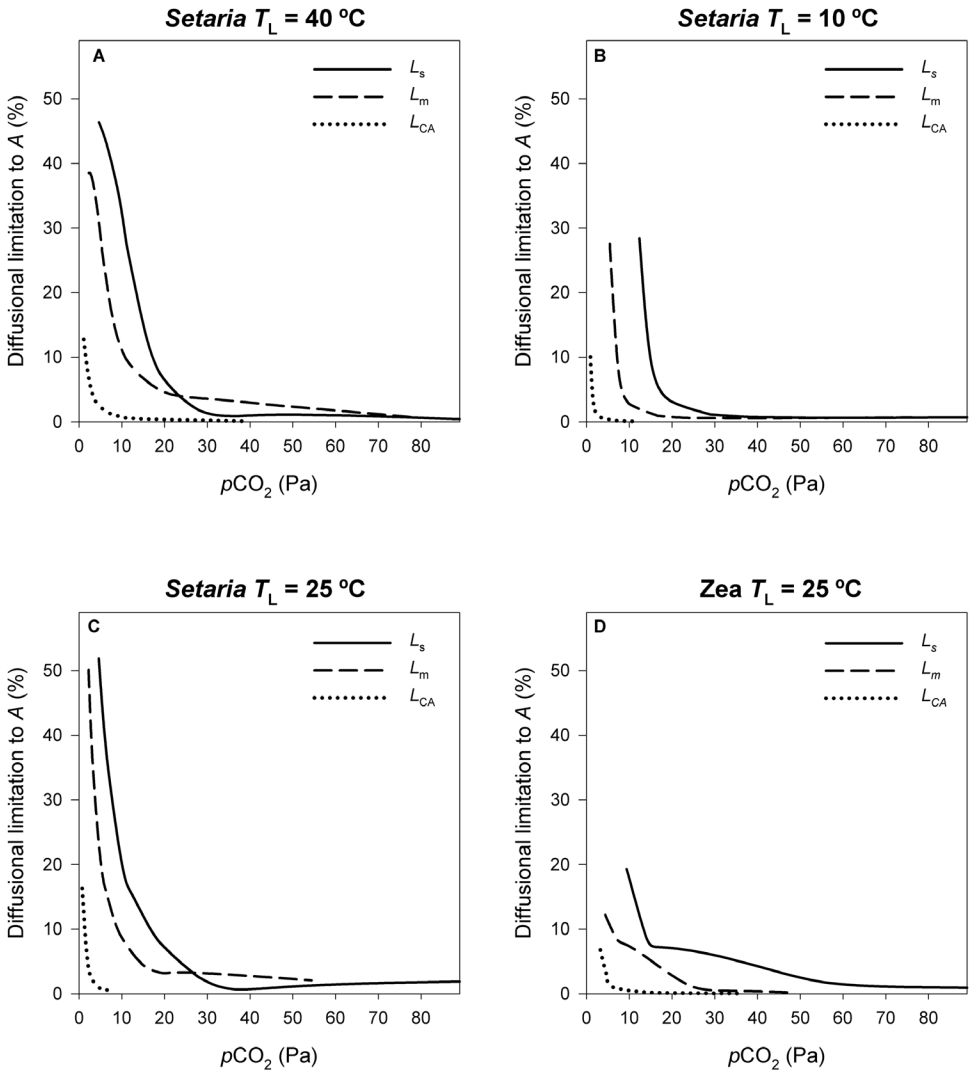

Fig. 4. Diffusional limitation to photosynthetic rate (*A*) imposed by stomatal resistance (L_s, Eqn 11, solid line), mesophyll resistance (L_m, Eqn 12, dashed line), and carbonic anhydrase (L_{CA}, Eqn 13, dotted line) as a function of the CO_2 supply (pCO_2) available for each (C_a, C_i, and C_m for L_s, L_m, and L_{CA}, respectively). (A) *Setaria viridis* at T_L=40 °C, (B) *Setaria viridis* at T_L=10 °C, (C) *Setaria viridis* at T_L=25 °C, and (D) *Zea mays* at T_L=25 °C.

Leakiness (ϕ)

Values of ϕ across pCO_2 for *Setaria* and *Zea* at 25 °C calculated under different modeling assumptions are shown in Fig. 5. When g_m was finite and variable with pCO_2 (Model 1), ϕ increased from low to high pCO_2, with a range of 0.16–0.59 in *Zea* and 0.45–0.76 in *Setaria*. Assuming that g_m was infinite and V_{pmax} variable with pCO_2 (Model 2) removed the pCO_2 response of ϕ and generally decreased ϕ at all pCO_2 in *Setaria*, but only at large pCO_2 in *Zea*. Model 3 resulted in nearly identical ϕ to Model 2 using the same finite g_m as Model 1 but with the solution constrained by only the photosynthesis model. However, this scenario failed to predict Δ^{13}_{obs} (see Supplementary Fig. S2). Imposing a PEP regeneration rate (V_{pr}) limitation of 64 and 59 μmol m^{-2} s^{-1} in *Setaria* and *Zea*, respectively (Model 4), decreased ϕ compared to the results with Model 1 in *Setaria* but resulted in no change in *Zea*. Interestingly, at pCO_2 ≤ambient air, values for ϕ were similar across models in *Zea*, but they differed in *Setaria*. The values of V_{pmax}, V_{cmax}, V_p, V_c, C_{bs}, and g_{bs} used in these four models are reported in Supplementary Fig. S2.

For comparison we also present ϕ at ambient pCO_2 calculated with the simplified Eqn 19 and assuming either g_m finite or infinite. For both species, ϕ calculated with Eqn 19 was not different to values obtained with the complete Eqn 16 when g_m was finite (compare black lines and black symbols in Fig. 5) and when g_m was infinite (compare grey dashed line and clear symbols).

Discussion

Calculation of mesophyll conductance and model parameterization

Mesophyll conductance (g_m) was derived with the *in vitro* V_{pmax} method (Ubierna *et al.*, 2017). Estimations of g_m with this method were similar to $\Delta^{18}O$-g_m across temperatures (Ubierna *et al.*, 2017) and across pCO_2 (Kolbe and Cousins, 2018). Potential errors in g_m originating from inaccurate model parameterization of the *in vitro* V_{pmax} method were tested with a sensitivity analysis using *Setaria* data at three

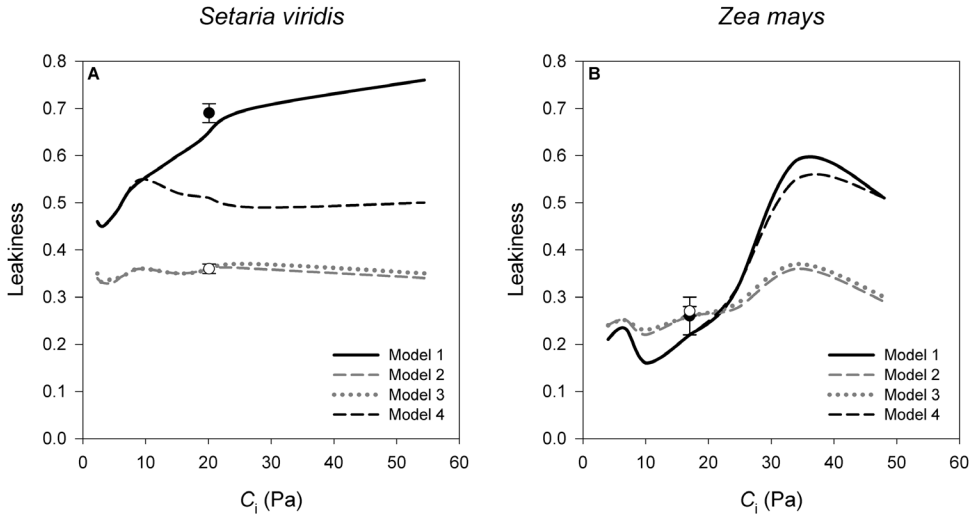

Fig. 5. Effect of different parameterizations of models of photosynthesis in the calculation of leakiness (ϕ) in (A) *Setaria virids* and (B) *Zea mays* at 25 °C and over a range of pCO_2 inside the leaf intercellular spaces (C_i). Model 1 (solid black line) uses *in vitro* V_{pmax} and g_m finite and equal to the values presented in Fig. 3; Model 2 (dashed grey line) uses *in vivo* V_{pmax} (which is variable with pCO_2, see Supplementary Fig. S2) and g_m infinite; Model 3 (dotted grey line) uses the same as Model 1 but the solution was only constrained by A and not $\Delta^{13}C$; Model 4 (dashed black line) uses the same as Model 1 but introducing V_{pr} (= 64 and 59 μmol m^{-2} s^{-1} in *Setaria* and *Zea*, respectively) in the calculation of V_p (Eqn 6). The rest of the variables included in these models were calculated as explained in the Methods section: values for some of them can be found in Supplementary Fig. S2. In Models 1, 2, and 4, ϕ was calculated with Eqns 14 or 16 (same result) and in Model 3, ϕ was calculated with Eqn 14. The symbols indicate the value of ϕ at ambient air pCO_2 calculated with the simplified Eqn 19 assuming either g_m finite (solid symbols) or infinite (clear symbols). Values are means ±SE; n=4 in *Setaria*, n=3 in *Zea*.

temperatures and across pCO_2 (see Supplementary Fig. S3). Halving *in vitro* V_{pmax} increased g_m by <20% at large pCO_2 and almost doubled it at low pCO_2 and high temperature. Alternatively, doubling *in vitro* V_{pmax} decreased g_m by <15% at all pCO_2 and temperatures (Supplementary Fig. S3J–L). This demonstrates that uncertainties in *in vitro* V_{pmax} affect absolute values of g_m, but not the trend of increasing g_m with decreasing pCO_2. The sensitivity analysis also demonstrated that variations up to ±50% in K_P, K_C, or K_{CA} resulted in negligible (when pCO_2 ≥ambient) or small (at low pCO_2) errors in g_m calculations at any temperature (Supplementary Fig. S3A–I) and did not affect the observed trend of g_m with pCO_2.

In C_3 plants, it has been suggested that large g_m values reported for low pCO_2 might be an artifact of uncertainties in parameters such as R_d, Γ*, and b'_3 (Gu and Sun, 2014). The simulations with different values for R_d (see Supplementary Fig. S4A, B) or b'_3 (Supplementary Fig. S4C, D) resulted in variations in g_m of <6% and did not affect the trend of increasing g_m with decreasing pCO_2. Ubierna *et al.* (2017) demonstrated that g_m is largely independent of values of g_{bs} or V_{cmax} and this is also illustrated in Supplementary Fig. S2.

CA-limited versus CA-saturated models to estimate g_m

The substrate for the initial carboxylation by PEPC is HCO_3^- and not CO_2. However, V_p is often calculated in terms of CO_2, because the hydration of CO_2 (V_h) generally happens very fast when catalysed by CA (Stryer, 1988). We refer to this case as the CA-saturated model. In contrast, the CA-limited model calculates V_p as a function of HCO_3^-. The value of HCO_3^- is calculated with C_m, V_h, V_{pmax}, and a series of rate constants (see Ubierna *et al.*, 2017, for details). Producing the same V_p with the CA-limited and the CA-saturated calculations requires larger C_m for the former than the latter, and the difference could potentially be large if V_h is low. Subsequently, neglecting the hydration step, as in the CA-saturated calculations, can result in under-estimation of C_m and g_m. The terminology CA-saturated or -limited refers to the modeling of V_p and how this affects the calculated C_m value, but it does not imply different roles of CA in the photosynthetic process. Ubierna *et al.* (2017) found no difference between CA-sat g_m and CA-lim g_m at ambient pCO_2; however, the aim here is to compare these calculations for a range of pCO_2.

In both species and at all temperatures, the difference between CA-sat g_m and CA-lim g_m was negligible for pCO_2 >ambient (Fig. 2). However, as pCO_2 decreased, CA-lim g_m became larger than CA-sat g_m, especially at high temperatures and in *Zea*. In this species ignoring the hydration step resulted in under-estimating g_m by as much as 20%, whereas in *Setaria* the under-estimation was <5%.

The larger differences at high temperatures can be explained by the temperature response of K_{CA}, which increases from 10 to 30 °C but plateaus above that (Boyd *et al.*, 2015). Species differences can be explained by different K_{CA} values and CO_2 availability to CA. Firstly, K_{CA} in *Setaria* (124 μmol m^{-2} s^{-1} Pa^{-1}) was double the value for *Zea* (65.5 μmol m^{-2} s^{-1} Pa^{-1}). Below ambient pCO_2, *Setaria* and *Zea* had similar A, g_s, and C_i. Sustaining similar A in these two species requires larger C_m in *Zea* than in *Setaria* because of the lower *in vitro* V_{pmax} value in the former (184 μmol m^{-2} s^{-1}) versus the latter (450 μmol m^{-2} s^{-1}). Therefore, in *Zea* the lower K_{CA} and *in vitro* V_{pmax} was counterbalanced by increased CO_2 availability to CA through higher g_m. Osborn *et al.* (2017) also suggested large g_m as a mechanism to increase CO_2 assimilation rate at low pCO_2.

At low pCO_2 or in species with low K_{CA}, ignoring the hydration step results in under-estimation of g_m. However, the error is insignificant at pCO_2 above ambient or in species with large K_{CA}, such as *Setaria*. The hydration step should be included for accurate determination of g_m at low pCO_2 in species with low K_{CA} and/or high A, such as C_4 grasses (Cousins *et al.*, 2008), especially at high temperatures.

Values for CA-lim g_m and variation with pCO_2

Across pCO_2 and temperatures, CA-lim g_m ranged from 0.6 ± 0.1 to 9.3 ± 1.5 μmol m^{-2} s^{-1} Pa^{-1} in *Setaria*, and 0.6 ± 0.1 to 16.2 ± 5.7 μmol m^{-2} s^{-1} Pa^{-1} in *Zea* (Fig. 3). In *Zea*, photosynthetic rate declined above ambient pCO_2, indicating deactivation at low C_i that did not fully recover when pCO_2 supply was returned to ambient levels (Fig. 1B). This could have introduced some bias in the CA-lim g_m values calculated at high pCO_2. Nevertheless, the CA-lim g_m values were used at pCO_2 ≤ambient, because above ambient, photosynthesis was not restricted by diffusional limitations (Fig. 4).

To validate CA-lim g_m values, they were compared with literature reports for the same species obtained with the alternative $\Delta^{18}O$ method (Barbour *et al.*, 2016; Osborn *et al.*, 2017; Ubierna *et al.*, 2017; Fig. 3). In *Zea*, there was a good agreement between $\Delta^{18}O$-g_m (Barbour *et al.*, 2016; Ubierna *et al.*, 2017) and CA-lim g_m (Fig. 3B). A recent study in *Zea* by Kolbe and Cousins (2018) also found agreement between $\Delta^{18}O$-g_m and *in vitro* V_{pmax} g_m across a range of pCO_2, although both estimations of g_m deviated at very low pCO_2. In *Setaria*, $\Delta^{18}O$-g_m (Barbour *et al.*, 2016; Osborn *et al.*, 2017; Ubierna *et al.*, 2017) was larger than our CA-lim g_m results (Fig. 3A–C). This discrepancy could have originated if *in vitro* V_{pmax} was over-estimated, and more studies exploring g_m variation and assessing the impacts of the method are needed.

In *Zea* at 25 °C and in *Setaria* at three temperatures, the CA lim-g_m increased with short-term exposure to decreasing pCO_2. Increasing g_m with decreasing pCO_2 has also been observed in C_3 species (Bongi and Loreto, 1989; Loreto *et al.*, 1992; Flexas *et al.*, 2007, 2008; Hassiotou *et al.*, 2009; Bunce, 2010; Douthe *et al.*, 2011; Tazoe *et al.*, 2011), although there are also a few studies that have concluded there is no change (Loreto *et al.*, 1992; Tazoe *et al.*, 2009). There are only two studies that have presented C_4-g_m across pCO_2. In Osborn *et al.* (2017), $\Delta^{18}O$-g_m values for *Setaria* increased with decreasing pCO_2 but the trend was not significant. In *Zea*, Kolbe and Cousins (2018) found a significant increase in $\Delta^{18}O$-g_m with decreasing pCO_2.

The initial slope of an A-C_i curve can be modified with either C_m (g_m) or V_{pmax} (see Supplementary Fig. S5). Therefore, there may be a value for V_{pmax} that would cancel out the trend in CA-lim g_m. However, this is not the case if V_{pmax} is independent of pCO_2, and cancelling the observed trend in CA-lim g_m would require V_{pmax} to decrease with increasing pCO_2 (Supplementary Fig. S6). There is evidence showing that CO_2 levels affect the phosphorylation state of PEPC and PEPCK, and therefore variation of *in vivo* V_{pmax} across pCO_2 could be expected (Bailey *et al.*, 2007). However, the CO_2 response of photosynthetic rate was found to be no different between wild-type and transgenic plants with low PEPC phosphorylation (Furumoto *et al.*, 2007). Much of the post-translational modifications that presumably lower V_{pmax} would probably occur when CO_2 is saturating and some other factor limits C_4 photosynthesis. At ambient pCO_2 and below it is generally thought, although not known, that PEPC is operating at V_{pmax}. The fact that $\Delta^{18}O$-g_m data have demonstrated a similar trend of increasing g_m with decreasing pCO_2 (Kolbe and Cousins, 2018) points to a constant V_{pmax} value. Nevertheless, if fast *in vivo* regulation of V_{pmax} occurs it could alter values and trends in g_m. In reality, there might be a combination of both fluctuations in g_m and V_{pmax} in response to short-term variation in pCO_2. Future work should investigate *in vivo* regulation of V_{pmax} and its impact on g_m calculations.

Limitation to photosynthesis at low pCO_2

C_4 photosynthesis saturates at ambient pCO_2 and A was not limited by diffusion, as indicated by L_s, L_m, and L_{CA} ≈ 0% for both species and all temperatures (Fig. 4). However, below ambient air pCO_2, diffusional limitations constrained CO_2 assimilation and increased exponentially with decreasing pCO_2. As shown in Fig. 1 and Supplementary Fig. S5, in both species the CO_2 responsive part of the A-C_i curve corresponded to C_i below ~10 Pa. This raises the question of whether C_4 plants operate below this threshold. In laboratory experiments, high irradiance and N fertilization shifted the operational C_i down to the CO_2 responsive part of the A-C_i curve (Ghannoum *et al.*, 1997; Ghannoum and Conroy, 1998). Additionally, moderate water stress decreased C_i in several C_4 species, although under severe drought declines in A precluded C_i from getting very low (Ghannoum, 2009, and references herein). Under ambient air pCO_2, C_i<11 Pa were reported for *Zea* grown in FACE-type experiments (Leakey *et al.*, 2004; Markelz *et al.*, 2011), and *Sorghum bicolor* grown in an open field reached C_i/C_a=0.2 after two consecutive water-stress cycles (Steduto *et al.*, 1997). Therefore, under certain growth conditions, CO_2 availability may limit C_4 photosynthesis.

Interestingly, *Setaria* and *Zea* displayed different behavior at low pCO_2. At low pCO_2, *Zea* was more efficient because it achieved high A despite lower V_{pmax} and K_{CA} by decreasing diffusional limitations and sustaining greater C_m with high g_m. The high g_m at low pCO_2 could increase or maintain photosynthesis at low C_i and could improve photosynthetic rates under situations that result in low CO_2 availability, such as drought.

In both species, the conversion of CO_2 into bicarbonate as catalysed by CA was fast enough that the hydration rate only limited A at low pCO_2 (L_{CA}=6–16% for C_m<4 Pa, Fig. 4). Such low C_m is unlikely to occur, even under drought conditions. At these very low pCO_2, the hydration rate (V_h) was comparable to rates in CA-depleted transgenic plants (Supplementary Fig. S7). For example, in *Setaria* at 25 °C, V_h decreased from 581 μmol m^{-2} s^{-1} at ambient pCO_2 to 100 μmol m^{-2} s^{-1} at the lowest pCO_2 measured. Using values from Osborn *et al.* (2017) at 25 °C and ambient pCO_2 to calculate V_h as $C_m \times K_{CA}$ resulted in 1215 and 142 μmol m^{-2} s^{-1}

for the wild type and CA-depleted transgenic, respectively. Osborn *et al.* (2017) concluded that in *Setaria* at low pCO_2, g_m posed a greater limitation than CA activity. Our study confirms that g_m is a major determinant of photosynthetic capacity at low pCO_2 and CA further constrains assimilation rates only at very low pCO_2. However, the CA limitation at low pCO_2 will be exacerbated at higher temperatures as the hydration rate is less able to keep up with the increase in PEPC activity (Boyd *et al.*, 2015).

Leakiness (ϕ)

Leakiness is often estimated from comparing models and measurements of $\Delta^{13}C$ assuming g_m is infinite (Pengelly *et al.*, 2010; Ubierna *et al.*, 2011, 2013) or large (Kromdijk *et al.*, 2010). Values of ϕ vary by as much as 0.04–0.9 (for a compilation of values and review of methods see Kromdijk *et al.*, 2014), although for most species under most conditions ϕ=0.2–0.3 (Cousins *et al.*, 2006; Kromdijk *et al.*, 2010; Pengelly *et al.*, 2010; Ubierna *et al.*, 2013; Bellasio and Griffiths, 2014).

In our study, considering g_m to be finite had a different effect on the calculation of ϕ for *Setaria* and *Zea*. At ambient air pCO_2 and 25 °C, both *Setaria* and *Zea* had similar g_m (2.00 and 2.43 μmol m^{-2} s^{-1} Pa^{-1}, respectively). However, while ϕ in *Zea* was the same whether g_m was finite or infinite, in *Setaria*, accounting for a finite g_m doubled ϕ (Fig. 5, compare Models 1 and 2). This high ϕ in *Setaria* was driven by constrains imposed by the $\Delta^{13}C$ model rather than the photosynthesis model. This is illustrated by the comparison of Models 2 and 3 (Fig 5). Both models predicted the same A and ϕ, but Model 2 used g_m finite (and *in vitro* V_{pmax}) and Model 3 assumed g_m infinite (and *in vivo* V_{pmax}). However, Model 3 failed to predict Δ^{13}_{obs} (see Supplementary Fig. S2). Forcing the solution to satisfy both models of A and Δ^{13}_{obs} resulted in increases in ϕ in *Setaria*, but not in *Zea*.

This can be explained through the relationship between $\Delta^{13}C$ and C_m/C_a, which is illustrated in Fig. 6 for different values of ϕ. Increasing C_m/C_a results in either increased or decreased $\Delta^{13}C$ depending on whether ϕ is low (≤0.3) or high (Henderson *et al.*, 1992; von Caemmerer *et al.*, 2014). When $\Delta^{13}_{obs} > a_s + (a_m - a_s)(C_i/C_a)$ (= 4.4–2.6 C_i/C_a ≈ 2.9‰ in our data set at 25 °C and ambient pCO_2) increasing C_m/C_a results in decreased ϕ; meanwhile the opposite is true when $\Delta^{13}_{obs} < 4.4 - 2.6\, C_i/C_a$. The value $a_s + (a_m - a_s)(C_i/C_a)$ represents the intercept of the line $\Delta^{13}C$ versus C_m/C_a when C_{bs} and boundary layer conductance are large and ternary effects are ignored. At ambient air pCO_2 and 25 °C, Δ^{13}_{obs} =3.1‰ in *Zea*. Therefore, varying C_m/C_a resulted in minimal changes in ϕ (compare black triangle and circle in Fig. 6). However, in *Setaria*, Δ^{13}_{obs} =4.5‰ and therefore low C_m/Ca translated into large ϕ (compare grey triangle and circle in Fig. 6). The photosynthesis model demonstrated that this increase in ϕ was achieved by increased V_p and g_{bs} (see Supplementary Fig. S2).

It is questionable that *Setaria* operates with ϕ=0.7, and it is seemly unreasonable that it does. Because $\Delta^{13}C$ is mostly determined by C_m/C_a and ϕ, low C_m/C_a forces the increase in ϕ. But are there any other parameters in the discrimination equation that could be manipulated in order to predict large $\Delta^{13}C$ with low C_m/C_a without large ϕ? Calculations of ϕ with the complete (Eqn 16) and simplified (Eqn 19) models suggest that, at least at ambient pCO_2, this was not the case. The simplified calculation of ϕ produced values similar to the complete model, suggesting that at ambient air pCO_2 or above, modifying parameters such as C_{bs}, b_3, or b_4 within their current definition did not result in large changes in $\Delta^{13}C$.

In addition to the possible post-translational regulation of V_{pmax}, PEP regeneration (V_{pr}) may also influence V_p (Eqn 6) and estimates of ϕ. In our calculations, V_{pr}=64 μmol m^{-2} s^{-1} decreased ϕ in *Setaria* by 0.3 and resulted in slightly larger g_m values at high pCO_2 but no change at low pCO_2 (compare Models 1 and 4 in Fig. 5 and Supplementary Fig. S2). In fact, at low pCO_2 it is expected that V_{pr} would not limit V_p and would have no effect on estimates of g_m or ϕ under these conditions. Changes in ϕ in response to pCO_2 or other conditions are possible if V_{pr} is allowed to vary, although at present V_{pr} variation across species, temperatures, or pCO_2 is unknown. The V_{pr} values that would be needed to remove the observed trend in g_m with pCO_2 are shown in Supplementary Fig. S8. Introducing a value for V_{pr} implies decoupling V_p from C_m (g_m). In other words, the required V_p value to support the measured A could be achieved by choosing the adequate V_{pr} rather than by varying C_m. This would also further complicate estimations of ϕ from $\Delta^{13}C$ as V_{pr} is not often measured and is not incorporated into the $\Delta^{13}C$ models.

Our calculations assume that theoretical models of photosynthesis and discrimination represent the actual photosynthetic

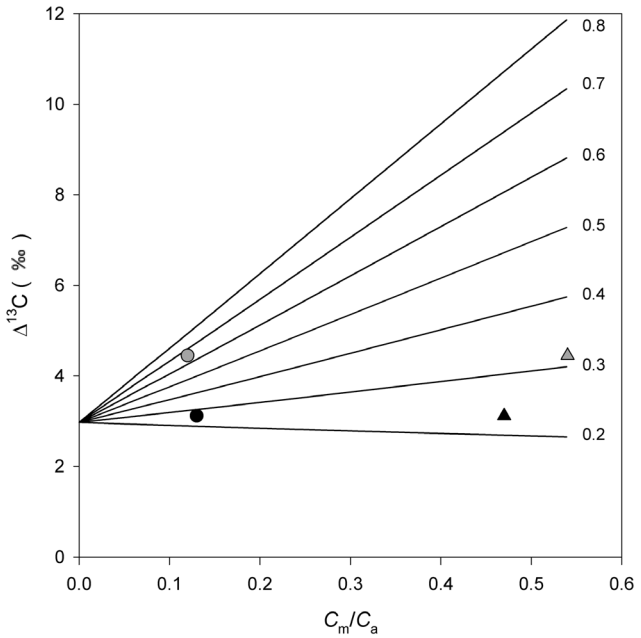

Fig. 6. $\Delta^{13}C$ (Eqn 9) as a function of C_m/C_a for different ϕ values (indicated by the numbers at the end of each line). For calculations we used values of 37, 36, 20, and 1364 Pa for C_a, C_L, C_i, and C_{bs}, respectively; t=0.0058, b_4=–4.49‰, and b_3=29.87‰. These values correspond to the mean values measured or calculated in *Setaria* at 25 °C and ambient pCO_2. Black symbols represent data for *Zea* and grey symbols for *Setaria*. For both species, ϕ was calculated assuming either g_m infinite (triangles) or g_m=2.00 and 2.43 μmol m^{-2} s^{-1} Pa^{-1} in *Setaria* and *Zea*, respectively (circles).

process; any inaccuracy in the models will introduce error in the calculated g_m. We have evaluated one common modelling simplification, the effect of CA limitation, and also the impact of uncertainty on input parameters. Additionally, we have used two contrasting species to illustrate the sensitivity of ϕ to g_m. Although a complete analysis of ϕ is beyond the scope of this work, this should be undertaken in future studies together with investigations on PEP regeneration limitations. Other future foci for research include: investigating *in vivo* and *in vitro* V_{pmax} values and variation across species and environmental conditions; and compiling leaf structure, CA, aquaporins, or other data that could reveal potential mechanisms behind observed g_m patterns.

Supplementary data

Supplementary data are available at *JXB* online.

Methods S1. Model of ^{13}C discrimination in C_4 species.

Table S1. Gas exchange values for C_i and A, and calculated values for C_m and CA-lim g_m in *Setaria viridis* and *Zea mays* at 25 °C and variable CO_2 supply.

Fig. S1. C_m across C_i in *Setaria viridis* at three temperatures, and in *Zea mays* at 25 °C.

Fig. S2. Description of the models used to evaluate the effect of g_m in calculations of ϕ.

Fig. S3. Sensitivity of calculations of CA-lim g_m in *Setaria viridis* to uncertainty in input parameters.

Fig. S4. Impact of R_d and b'_3 in the calculation of CA-lim g_m in *Setaria viridis* at 25 °C.

Fig. S5. Measured versus modeled response of A to C_i at 25 °C in *Setaria viridis* and *Zea mays* for different values of V_{pmax} and g_m.

Fig. S6. Values for *in vivo* V_{pmax} across C_i in *Setaria viridis* calculated when CA-lim g_m is constant with pCO_2.

Fig. S7. V_h across C_i in *Setaria viridis* at three temperatures.

Fig. S8. Values for V_{pr} across C_i in *Setaria viridis* calculated when CA-lim g_m is constant with pCO_2.

Acknowledgments

This research was supported by the Division of Chemical Sciences, Geosciences and Biosciences, Office of Basic Energy Sciences, Photosynthetic Systems through DE-SC0001685 and with instrumentation from an NSF Major Research Instrumentation grant #0923562. We thank an anonymous reviewer for valuable comments that improved this manuscript.

References

Arnau J, Bono R, Vallejo G. 2009. Analyzing small samples of repeated measures data with the mixed-model adjusted *F* test. Communications in Statistics - Simulation and Computation **38,** 1083–1103.

Bailey KJ, Gray JE, Walker RP, Leegood RC. 2007. Coordinate regulation of phosphoenolpyruvate carboxylase and phosphoenolpyruvate carboxykinase by light and CO_2 during C_4 photosynthesis. Plant Physiology **144,** 479–486.

Barbour MM, Evans JR, Simonin KA, von Caemmerer S. 2016. Online CO_2 and H_2O oxygen isotope fractionation allows estimation of mesophyll conductance in C_4 plants, and reveals that mesophyll conductance decreases as leaves age in both C_4 and C_3 plants. New Phytologist **210,** 875–889.

Bellasio C, Griffiths H. 2014. Acclimation to low light by C_4 maize: implications for bundle sheath leakiness. Plant, Cell & Environment **37,** 1046–1058.

Bongi G, Loreto F. 1989. Gas-exchange properties of salt-stressed olive (*Olea europea* L.) leaves. Plant Physiology **90,** 1408–1416.

Boyd RA, Gandin A, Cousins AB. 2015. Temperature responses of C_4 photosynthesis: biochemical analysis of Rubisco, phosphoenolpyruvate carboxylase, and carbonic anhydrase in *Setaria viridis*. Plant Physiology **169,** 1850–1861.

Bunce JA. 2010. Variable responses of mesophyll conductance to substomatal carbon dioxide concentration in common bean and soybean. Photosynthetica **48,** 507–512.

Cousins AB, Badger MR, von Caemmerer S. 2006. Carbonic anhydrase and its influence on carbon isotope discrimination during C_4 photosynthesis. Insights from antisense RNA in *Flaveria bidentis*. Plant Physiology **141,** 232–242.

Cousins AB, Badger MR, von Caemmerer S. 2008. C_4 photosynthetic isotope exchange in NAD-ME- and NADP-ME-type grasses. Journal of Experimental Botany **59,** 1695–1703.

Douthe C, Dreyer E, Epron D, Warren CR. 2011. Mesophyll conductance to CO_2, assessed from online TDL-AS records of $^{13}CO_2$ discrimination, displays small but significant short-term responses to CO_2 and irradiance in *Eucalyptus* seedlings. Journal of Experimental Botany **62,** 5335–5346.

Edwards GE, Walker DA. 1983. C_3, C_4: Mechanisms, and cellular and environmental regulation of photosynthesis. Oxford, UK: Blackwell Scientific Publications.

Evans JR. 1983. Nitrogen and photosynthesis in the flag leaf of wheat (*Triticum aestivum* L.). Plant Physiology **72,** 297–302.

Evans JR, Sharkey TD, Berry JA, Farquhar GD. 1986. Carbon isotope discrimination measured concurrently with gas exchange to investigate CO_2 diffusion in leaves of higher plants. Australian Journal of Plant Physiology **13,** 281–292.

Evans JR, Terashima I. 1988. Photosynthetic characteristics of spinach leaves grown with different nitrogen treatments. Plant and Cell Physiology **29,** 157–165.

Evans JR, von Caemmerer S. 1996. Carbon dioxide diffusion inside leaves. Plant Physiology **110,** 339–346.

Farquhar GD. 1983. On the nature of carbon isotope discrimination in C_4 species. Australian Journal of Plant Physiology **10,** 205–226.

Farquhar GD, Cernusak LA. 2012. Ternary effects on the gas exchange of isotopologues of carbon dioxide. Plant, Cell & Environment **35,** 1221–1231.

Farquhar GD, Sharkey TD. 1982. Stomatal conductance and photosynthesis. Annual Review of Plant Physiology **33,** 317–345.

Flexas J, Diaz-Espejo A, Galmés J, Kaldenhoff R, Medrano H, Ribas-Carbo M. 2007. Rapid variations of mesophyll conductance in response to changes in CO_2 concentration around leaves. Plant, Cell & Environment **30,** 1284–1298.

Flexas J, Ribas-Carbó M, Diaz-Espejo A, Galmés J, Medrano H. 2008. Mesophyll conductance to CO_2: current knowledge and future prospects. Plant, Cell & Environment **31,** 602–621.

Furumoto T, Izui K, Quinn V, Furbank RT, von Caemmerer S. 2007. Phosphorylation of phosphoenolpyruvate carboxylase is not essential for high photosynthetic rates in the C_4 species *Flaveria bidentis*. Plant Physiology **144,** 1936–1945.

Ghannoum O. 2009. C_4 photosynthesis and water stress. Annals of Botany **103,** 635–644.

Ghannoum O, Conroy JP. 1998. Nitrogen deficiency precludes a growth response to CO_2 enrichment in C_3 and C_4 *Panicum* grasses. Australian Journal of Plant Physiology **25,** 627–636.

Ghannoum O, von Caemmerer S, Barlow EWR, Conroy JP. 1997. The effect of CO_2 enrichment and irradiance on the growth, morphology and gas exchange of a C_3 (*Panicum laxum*) and a C_4 (*Panicum antidotale*) grass. Australian Journal of Plant Physiology **24,** 227–237.

Gillon JS, Yakir D. 2000a. Internal conductance to CO_2 diffusion and $C^{18}OO$ discrimination in C_3 leaves. Plant Physiology **123,** 201–214.

Gillon JS, Yakir D. 2000b. Naturally low carbonic anhydrase activity in C_4 and C_3 plants limits discrimination against $C^{18}OO$ during photosynthesis. Plant, Cell & Environment **23,** 903–915.

Gu L, Sun Y. 2014. Artefactual responses of mesophyll conductance to CO_2 and irradiance estimated with the variable *J* and online isotope discrimination methods. Plant, Cell & Environment **37,** 1231–1249.

Hassiotou F, Ludwig M, Renton M, Veneklaas EJ, Evans JR. 2009. Influence of leaf dry mass per area, CO_2, and irradiance on mesophyll conductance in sclerophylls. Journal of Experimental Botany **60,** 2303–2314.

Hatch MD. 1987. C_4 photosynthesis: a unique blend of modified biochemistry, anatomy and ultrastructure. Biochemical and Biophysical Acta **895,** 81–106.

Hatch MD, Burnell JN. 1990. Carbonic anhydrase activity in leaves and its role in the first step of C_4 photosynthesis. Plant Physiology **93,** 825–828.

Hatch MD, Slack CR, Johnson HS. 1967. Further studies on a new pathway of photosynthetic carbon dioxide fixation in sugar-cane and its occurrence in other plant species. The Biochemical Journal **102,** 417–422.

Henderson SA, von Caemmerer S, Farquhar GD. 1992. Short-term measurements of carbon isotope discrimination in several C_4 species. Australian Journal of Plant Physiology **19,** 263–285.

Jenkins CL, Furbank RT, Hatch MD. 1989. Mechanism of C_4 photosynthesis: a model describing the inorganic carbon pool in bundle sheath cells. Plant Physiology **91,** 1372–1381.

Kolbe AR, Cousins AB. 2018. Mesophyll conductance in *Zea mays* responds transiently to CO_2 availability: implications for transpiration efficiency in C_4 crops. New Phytologist. In press. doi:10.1111/nph.14942.

Kromdijk J, Griffiths H, Schepers HE. 2010. Can the progressive increase of C_4 bundle sheath leakiness at low PFD be explained by incomplete suppression of photorespiration? Plant, Cell & Environment **33,** 1935–1948.

Kromdijk J, Ubierna N, Cousins AB, Griffiths H. 2014. Bundle-sheath leakiness in C_4 photosynthesis: a careful balancing act between CO_2 concentration and assimilation. Journal of Experimental Botany **65,** 3443–3457.

Leakey ADB, Bernacchi CJ, Dohleman FG, Ort DR, Long SP. 2004. Will photosynthesis of maize (*Zea mays*) in the US Corn Belt increase in future [CO_2] rich atmospheres? An analysis of diurnal courses of CO_2 uptake under free-air concentration enrichment (FACE). Global Change Biology **10,** 951–962.

Loreto F, Harley PC, Di Marco G, Sharkey TD. 1992. Estimation of mesophyll conductance to CO_2 flux by three different methods. Plant Physiology **98,** 1437–1443.

Markelz RJ, Strellner RS, Leakey AD. 2011. Impairment of C_4 photosynthesis by drought is exacerbated by limiting nitrogen and ameliorated by elevated [CO_2] in maize. Journal of Experimental Botany **62,** 3235–3246.

Osborn HL, Alonso-Cantabrana H, Sharwood RE, Covshoff S, Evans JR, Furbank RT, von Caemmerer S. 2017. Effects of reduced carbonic anhydrase activity on CO_2 assimilation rates in *Setaria viridis*: a transgenic analysis. Journal of Experimental Botany **68,** 299–310.

Peisker M. 1986. Models of carbon metabolism in C_3–C_4 intermediate plants as applied to the evolution of C_4 photosyntheis. Plant, Cell & Environment **9,** 627–635.

Peisker M, Henderson SA. 1992. Carbon: terrestrial C_4 plants. Plant, Cell & Environment **15,** 987–1004.

Pengelly JJ, Sirault XR, Tazoe Y, Evans JR, Furbank RT, von Caemmerer S. 2010. Growth of the C_4 dicot *Flaveria bidentis*: photosynthetic acclimation to low light through shifts in leaf anatomy and biochemistry. Journal of Experimental Botany **61,** 4109–4122.

Sage RF. 2004. The evolution of C_4 photosynthesis. New Phytologist **161,** 341–370.

Steduto P, Katerji N, Puertos-Molina H, Ünlü M, Mastrorilli M, Rana G. 1997. Water-use efficiency of sweet sorghum under water stress conditions. Gas-exchange investigations at leaf and canopy scales. Field Crops Research **54,** 221–234.

Stryer L. 1988. Biochemistry. New York: W. H. Freeman.

Tazoe Y, von Caemmerer S, Badger MR, Evans JR. 2009. Light and CO_2 do not affect the mesophyll conductance to CO_2 diffusion in wheat leaves. Journal of Experimental Botany **60,** 2291–2301.

Tazoe Y, von Caemmerer S, Estavillo GM, Evans JR. 2011. Using tunable diode laser spectroscopy to measure carbon isotope discrimination and mesophyll conductance to CO_2 diffusion dynamically at different CO_2 concentrations. Plant, Cell & Environment **34,** 580–591.

Tholen D, Ethier G, Genty B, Pepin S, Zhu XG. 2012. Variable mesophyll conductance revisited: theoretical background and experimental implications. Plant, Cell & Environment **35,** 2087–2103.

Tholen D, Zhu XG. 2011. The mechanistic basis of internal conductance: a theoretical analysis of mesophyll cell photosynthesis and CO_2 diffusion. Plant Physiology **156,** 90–105.

Ubierna N, Gandin A, Boyd RA, Cousins AB. 2017. Temperature response of mesophyll conductance in three C4 species calculated with two methods: ^{18}O discrimination and in vitro V_{pmax}. New Phytologist **214,** 66–80. Corrigendum. New Phytologist 217: 956–959.

Ubierna N, Sun W, Cousins AB. 2011. The efficiency of C_4 photosynthesis under low light conditions: assumptions and calculations with CO_2 isotope discrimination. Journal of Experimental Botany **62,** 3119–3134.

Ubierna N, Sun W, Kramer DM, Cousins AB. 2013. The efficiency of C_4 photosynthesis under low light conditions in *Zea mays*, *Miscanthus* × *giganteus* and *Flaveria bidentis*. Plant, Cell & Environment **36,** 365–381.

von Caemmerer S. 2000. Biochemical models of leaf photosynthesis. Collingwood, Australia: CSIRO publishing.

von Caemmerer S, Ghannoum O, Pengelly JJ, Cousins AB. 2014. Carbon isotope discrimination as a tool to explore C_4 photosynthesis. Journal of Experimental Botany **65,** 3459–3470.

Warren CR. 2008. Stand aside stomata, another actor deserves centre stage: the forgotten role of the internal conductance to CO_2 transfer. Journal of Experimental Botany **59,** 1475–1487.

Warren CR, Ethier GJ, Livingston NJ, Grant NJ, Turpin DH, Harrison DL, Black TA. 2003. Transfer conductance in second growth Douglas-fir (*Pseudotsuga menziesii* (Mirb.) Franco) canopies. Plant, Cell & Environment **26,** 1215–1227.

Yin X, van der Putten PE, Driever SM, Struik PC. 2016. Temperature response of bundle-sheath conductance in maize leaves. Journal of Experimental Botany **67,** 2699–2714.